Catalysis Science & Technology

ROYAL SOCIETY OF CHEMISTRY

PAPER

View Article Online
View Journal | View Issue

Cite this: *Catal. Sci. Technol.*, 2025, 15, 6135

Near-infrared isomeric polymerized small molecular acceptors with thiophene-fused end groups for efficient photocatalytic hydrogen evolution

Jingcheng Zhao,[ab] Mengqi Cao,[ab] Yulu Liu,[ab] Panpan Wang,[ab] Xiaofu Wu,[a] Hui Tong *[ab] and Lixiang Wang *[ab]

Polymerized small molecular acceptors (PSMAs) now represent a class of promising organic photocatalysts for efficient photocatalytic hydrogen evolution due to their outstanding visible and near-infrared (NIR) light absorption. Although the isomerization strategy has been recognized as a simple yet effective method to modulate photovoltaic properties of PSMAs, the effects of isomerization on the performance of photocatalytic hydrogen evolution have never been reported so far. Herein, two isomeric thiophene-fused electron-withdrawing end groups with different fused sites are applied to construct isomeric PSMAs without π-linking units, namely **PY-*α*-CPTCN** and **PY-*β*-CPTCN**. Despite possessing identical molecular formulas, their π-conjugation and charge distribution are highly sensitive to the substitution patterns of thiophene-fused terminal units. Combined with experimental analysis and theoretical calculation, **PY-*α*-CPTCN** exhibits more efficient light absorption and charge transport than that of **PY-*β*-CPTCN**, ascribed to its stronger intramolecular π-conjugation effect. The resulting photocatalyst based on **PY-*α*-CPTCN** displays an average hydrogen evolution rate of 252.2 mmol g^{-1} h^{-1} under AM 1.5 G sunlight (100 mW cm^{-2}), which is 3.2 times higher than that of **PY-*β*-CPTCN** with 79.7 mmol g^{-1} h^{-1}. These results not only reveal the isomerization strategy as an effective method for the design of high-performance PSMA-based photocatalysts, but also emphasize the relevance between the intramolecular π-conjugation and photocatalytic properties.

Received 26th June 2025,
Accepted 21st August 2025

DOI: 10.1039/d5cy00775e

rsc.li/catalysis

Introduction

The growing energy demands in modern society as well as severe challenges of global climate change that result from extravagant consumption of fossil fuel energy have stimulated significant attention on sustainable energy harvest/conversion technologies.[1–5] Hydrogen is regarded as an ideal energy carrier, distinguished by its exceptional gravimetric energy density and completely carbon-free combustion process.[6,7] Solar-driven hydrogen evolution reaction, capable of producing hydrogen from water molecules under solar irradiation, has demonstrated remarkable potential *via* developing advanced semiconductor photocatalysts.[8,9] Specifically, organic semiconductors exhibited excellent light-harvesting capabilities and tunable optoelectronic properties through facile structural design, and garnered substantial research interest as alternatives to traditional inorganic counterparts.[10–13]

Overcoming the current bottleneck in photocatalytic water splitting systems requires optimizing light harvesting across the visible and near-infrared (NIR) spectral regions, which constitute approximately 70% of the solar spectrum.[14] Organic semiconductors have extended π-conjugation and tunable donor–acceptor (D–A) configurations, which can modulate optical absorption properties efficiently.[15,16] From this perspective, polymerized small-molecule acceptors (PSMAs) are highly competitive candidate materials in application of photocatalytic hydrogen evolution. PSMAs integrate π-conjugated main chains and multiple intramolecular D–A interactions, exhibiting outstanding performance in visible and NIR light-driven photocatalytic hydrogen evolution. For instance, Chou *et al.* reported that PSMA-based photocatalysts could broaden light absorption in the NIR region while maintaining efficient charge separation *via* regulating π-linkers between the small-molecule acceptors (SMAs) to achieve a high-performance photocatalytic reaction.[17] Recently, we synthesized a series of PSMA-based photocatalysts featuring varied π-linker

[a] *State Key Laboratory of Polymer Science and Technology, Changchun Institute of Applied Chemistry, Chinese Academy of Sciences, Changchun, 130022, China. E-mail: chemtonghui@ciac.ac.cn*
[b] *University of Science and Technology of China, Hefei, 230026, China*

lengths (thiophene, bithiophene, and terthiophene) and found that increasing the number of thiophene units can modulate the intramolecular charge transfer, which is a key factor for governing photocatalytic hydrogen evolution performance.[18] Overall, most of the research about PSMA-based photocatalysts primarily focuses on designing π-linker units and investigating their linker-dependent photocatalytic activity. Compared with PSMAs with π-linkers, simple PSMAs without π-linkers can reflect the role of SMA units in PSMAs more intuitively, which helps to understand the influence of intramolecular charge transfer and π-conjugation effect of SMA units on the intrinsic properties of PSMAs. However, the relationship between the structure and the photocatalytic performance of PSMAs without any linking units remains inadequately explored so far.

The electron-withdrawing end groups of SMAs play a crucial role in determining their electron affinity, light absorption, energy levels and intermolecular interactions.[19,20] Phenyl- or thienyl-fused end groups with bromine atoms on benzene or thiophene rings are frequently employed in the construction of PSMAs.[21,22] Compared to the phenyl-fused end groups in PSMAs, thienyl-fused end groups can reduce steric hindrance, leading to enhanced electron delocalization and intermolecular interactions for PSMAs. Among various strategies for modulating end groups, the isomerization of end groups is convenient and popular in the development of PSMAs for efficient all-polymer solar cells.[23,24] Altering the spatial arrangements or linking positions within the homologous molecular skeleton significantly influences the molecular orbital distribution, thereby exerting substantial effects on the intrinsic electronic structures and intermolecular interactions. Specifically, the unique regio-isomeric phenomenon was often presented by the non-centrosymmetric thiophene rings due to the substitution-pattern and fused-site sensitivity, stemming from the high electron density and polarization on the sulfur atom.[25–27] The effect of isomeric thienyl-fused end groups of PSMAs has been demonstrated to regulate the photovoltaic performance efficiently, however, such an effect in photocatalytic hydrogen evolution has never been explored until now.[28–31]

In this context, two PSMAs without a π-linker unit (namely, **PY-*α*-CPTCN** and **PY-*β*-CPTCN**) based on two isomeric SMAs featuring different thienyl-fused end groups are designed and synthesized, which offer an opportunity to study systematically and gain a deep insight into the roles of isomeric PSMAs in photocatalytic hydrogen evolution for the first time. As revealed by experimental results and theoretical calculation, although **PY-*β*-CPTCN** possesses a more rigid and planar molecular backbone, **PY-*α*-CPTCN** exhibits more delocalized and efficient intramolecular π-conjugation, leading to its improved light absorption and charge transport. In the photocatalytic experiment, the average hydrogen evolution rate (HER) of the **PY-*α*-CPTCN** photocatalyst is up to 252.2 mmol g^{-1} h^{-1} under simulated sunlight irradiation, while the HER of the **PY-*β*-CPTCN** catalyst is only 79.7 mmol g^{-1} h^{-1}. This work highlights the effectiveness of the isomerization strategy in the design of PSMA-type photocatalysts.

Results and discussion

The chemical structures and synthetic routes are presented in Fig. 1a and Scheme S1, respectively. Two isomeric thienyl-fused end groups (CPTCN) with bromine atoms at *α*- and *β*- positions of thiophene, respectively, were synthesized according to previously documented methods.[31,32] The dibrominated monomers Y-*α*-CPTCNBr and Y-*β*-CPTCNBr were obtained through Lewis acid-catalyzed Knoevenagel condensation reactions.[33,34] Their structures are confirmed by NMR and mass spectra (SI). The dibrominated monomers were bonded together under Stille–Kelly conditions by using Me_6Sn_2 to obtain the final polymers **PY-*α*-CPTCN** and **PY-*β*-CPTCN**. The number-average molecular weights (M_n) of **PY-*α*-CPTCN** and **PY-*β*-CPTCN** are found to be 23.3 and 17.1 kDa, with polydispersity (PDI) of 1.97 and 1.84, as characterized by gel permeation chromatography (GPC). As revealed by thermogravimetric analysis (TGA) (Fig. S1), the decomposition temperatures (T_d) of **PY-*α*-CPTCN** (366 °C) and **PY-*β*-CPTCN** (360 °C) are close due to the isomeric chemical structures. Both PSMAs are soluble in common organic solvents (*e.g.*, chloroform and chlorobenzene) at room temperature, and they can be processed into nanoparticles (NPs) easily using the mini-emulsion method.[35]

The UV-vis absorption spectra of the two PSMAs were surveyed in dilute solution and nanoparticle aqueous dispersion to investigate their photophysical characteristics (Fig. 1b, c and Table S1). As shown in Fig. 1b, the solution absorption maxima (λ_{max}) are located at 742 nm for **PY-*α*-CPTCN** and 760 nm for **PY-*β*-CPTCN**. **PY-*α*-CPTCN** and **PY-*β*-CPTCN** exhibit absorption onsets at 806 nm and 802 nm, corresponding to the optical band gaps of 1.54 eV and 1.55 eV, respectively. It is observed that the absorption spectra of their nanoparticle aqueous dispersions afford some changes in water when these PSMAs are blended with sodium 2-(3-thienyl)ethyloxybutylsulfonate

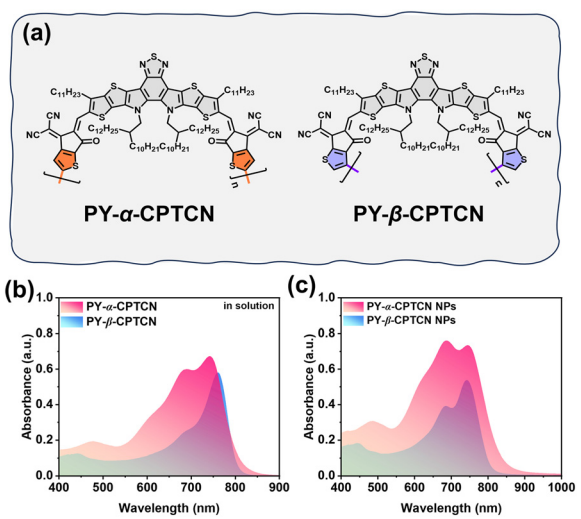

Fig. 1 (a) Chemical structures of PY-*α*-CPTCN and PY-*β*-CPTCN, respectively. (b) UV-vis absorption spectra of PY-*α*-CPTCN and PY-*β*-CPTCN in chloroform solution (6.25 μg mL^{-1}). (c) UV-vis absorption spectra of nanoparticles in aqueous dispersion (10 μg mL^{-1}).

(TEBS) (Fig. 1c). The absorption peak of **PY-α-CPTCN** NPs is located at 688 nm with a low-energy absorption at 744 nm, while **PY-β-CPTCN** NPs maintains the low-energy absorption peak at 742 nm. Moreover, the values of full width at half maximum (FHWM) at the strongest absorption band were measured to be 210 nm for **PY-α-CPTCN** NPs and 129 nm for **PY-β-CPTCN** NPs (Table S1), suggesting that **PY-α-CPTCN** NPs hold a broader absorption band in both visible and near-infrared regions. It is also clearly shown in Fig. 1c that the absorbance of **PY-α-CPTCN** NPs is integrally higher than that of **PY-β-CPTCN** NPs at the same concentration. The highest maximum extinction coefficients are 7.6×10^4 g^{-1} cm^{-1} for **PY-α-CPTCN** NPs and 5.4×10^4 g^{-1} cm^{-1} for **PY-β-CPTCN** NPs, respectively. Compared to the absorption spectra of PSMAs in chloroform solution, the PSMA nanoparticles in aqueous dispersion exhibit shifted absorption peaks with enhanced shoulder peaks, which may be attributed to changes in intermolecular aggregation originating from alterations in the solvent environment as well as the interactions between PMSAs and the stabilizing surfactant. In principle, the improved light absorption capacities of **PY-α-CPTCN** in both solution and NP states indicate its greater potential in photocatalytic hydrogen evolution.

Cryo-transmission electron microscopy (Cryo-TEM) and scanning electron microscopy (SEM) imaging of **PY-α-CPTCN** and **PY-β-CPTCN** NPs provide similar morphology with the particle size ranging from 10 to 110 nm (Fig. S4a, b and S5). The hydrodynamic diameter of nanoparticles was measured by dynamic light scattering (DLS), and the peak values of the *Z*-average particle size were estimated to be 78.8 nm for **PY-α-CPTCN** NPs and 91.3 nm for **PY-β-CPTCN** NPs (Fig. S6a). The zeta-potentials of **PY-α-CPTCN** NPs and **PY-β-CPTCN** NPs are −32.3 mV and −31.2 mV, thereby ensuring their good dispersity in water. As shown in Fig. S4c and d, the Pt-cocatalyst was deposited on the surface of nanoparticles as small dark particles with almost uniform particle size. The hydrophobic property of these PSMAs results in weak interactions between the photocatalysts and water molecules. The Pt particles on the nanoparticle surface may not only trap electrons from the light harvesting in PSMAs, but also provide the effective catalytic proton reduction sites. Interestingly, the Pt-particles were distributed evenly on the **PY-α-CPTCN** NPs, while uneven and patchy distribution of Pt-particles on the surface of **PY-β-CPTCN** NPs was observed. Considering the same nucleation and growth mechanism, the different morphology of Pt-particle deposition may also reflect that the PSMA phases exposed on the surface of **PY-α-CPTCN** NPs and **PY-β-CPTCN** NPs are different.[36]

To evaluate the catalytic activity, photocatalytic hydrogen evolution experiments of **PY-α-CPTCN** and **PY-β-CPTCN** photocatalysts were conducted initially under simulated sunlight irradiation (AM 1.5G, 100 mW cm^{-2}). In a typical photocatalytic process, the reaction medium consisted of 50 mL water with 0.2 M sacrificial electron donor (ascorbic acid). As shown in Fig. S8, the **PY-α-CPTCN** catalyst demonstrates better photocatalytic performance as expected. And there is no doubt that the contents of surfactant, photo-deposited Pt and nanoparticles of the sample have great impacts on the catalytic activity (Fig. S9–S11). Under optimized conditions of 0.1 wt% TEBS and 30 wt% Pt ratio loadings, the **PY-α-CPTCN** catalyst provides an average HER of 252.2 mmol g^{-1} h^{-1}, which is 3.2 times higher than that of the **PY-β-CPTCN** catalyst (79.7 mmol g^{-1} h^{-1}) (Fig. 2a). As shown in Fig. 2b, the absolute HER is initially elevated when increasing the catalyst mass, and reaches 174.0 μmol h^{-1} by using 1 mg **PY-α-CPTCN** NPs (20 μg mL^{-1}). However, a further increase of catalyst mass diminishes photocatalytic performance owing to the almost saturated light absorption and increased scattering.[37] As shown in Fig. S12, the apparent quantum yields (AQYs) of **PY-α-CPTCN** and **PY-β-CPTCN** catalysts were investigated under monochromatic incident light. The measured values of the **PY-α-CPTCN** catalyst comprehensively surpass those of the **PY-β-CPTCN** catalyst, further confirming its superior photocatalytic hydrogen evolution capability. Moreover, the **PY-α-CPTCN** catalyst maintains exceptional stability, showing negligible activity loss over six consecutive photocatalytic cycles (Fig. 2c), and its stable nanostructure could still be demonstrated by DLS even after prolonged reaction periods (Fig. S6b).

Cyclic voltammetry (CV) was conducted to estimate the highest occupied molecular orbital (HOMO) and the lowest

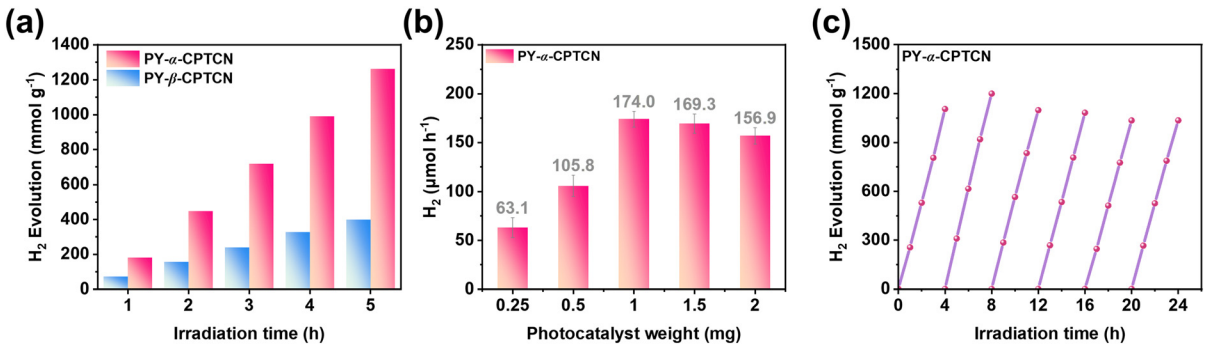

Fig. 2 (a) Hydrogen evolution *versus* time of **PY-α-CPTCN** and **PY-β-CPTCN** NPs at the concentration of 5 μg mL^{-1}, under AM 1.5G (100 mW cm^{-2}). (b) Photocatalytic H_2 evolution patterns of **PY-α-CPTCN** NPs with different weights of the photocatalyst. (c) Time course hydrogen evolution curve of **PY-α-CPTCN** NPs.

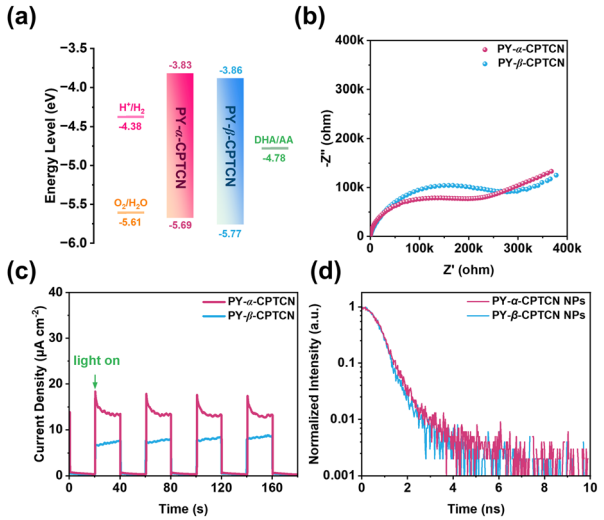

Fig. 3 (a) Energy level alignment of the redox potential of **PY-α-CPTCN** and **PY-β-CPTCN**. (b) Electrochemical impedance spectra of these materials. (c) Transient current density *vs.* time under intermittent light irradiation. (d) Transient PL decay spectra of **PY-α-CPTCN** and **PY-β-CPTCN** NPs.

unoccupied molecular orbital (LUMO) energy levels of the two PSMAs. As shown in Fig. 3a, the HOMO/LUMO levels of **PY-α-CPTCN** and **PY-β-CPTCN** were calculated to be −5.69/−3.83 eV and −5.77/−3.86 eV by analyzing their oxidation and reduction potentials (Fig. S13), confirming the ability of electron transfer between the PSMAs and co-catalyst. Their photoelectrochemical properties were evaluated by electrochemical impedance spectroscopy (EIS) and transient photocurrent measurements. As shown in Fig. 3b, **PY-α-CPTCN** has a smaller semicircle radius than **PY-β-CPTCN** in the EIS spectra, indicating a lower charge transfer resistance in **PY-α-CPTCN**. As proof, the **PY-α-CPTCN** photoelectrode exhibits a higher photocurrent response upon periodically switching the photoirradiation on and off, which is attributed its better exciton dissociation and charge transport (Fig. 3c). In addition, time-resolved photoluminescence (TRPL) spectra were obtained to estimated their fluorescence lifetimes. As shown in Fig. 3d, the PL decay profiles indicate that the average fluorescence lifetimes of **PY-α-CPTCN** NPs (1.00 ns) and **PY-β-CPTCN** NPs (0.81 ns) are comparable. Furthermore, the steady-state photoluminescence (PL) spectra (Fig. S14) demonstrate comparable emission intensities for both **PY-α-CPTCN** and **PY-β-CPTCN** NPs, indicating their similar radiative recombination characteristics. Consequently, the enhanced photocatalytic hydrogen evolution efficiency of **PY-α-CPTCN** is likely to be attributable to its superior light absorption capacity and charge transport properties.

To gain an in-depth understanding of the substantial difference between **PY-α-CPTCN** and **PY-β-CPTCN**, density functional theory (DFT) and time-dependent density functional theory (TD-DFT) calculations are performed. The calculated HOMO/LUMO levels are −5.68/−3.66 eV and −5.73/−3.70 eV for **PY-α-CPTCN** and **PY-β-CPTCN**, respectively (Table S1), which are consistent with the experimental results. Furthermore, the oscillator strengths (f) of $S_0 \rightarrow S_1$ transition were estimated to be 3.08 for **PY-α-CPTCN** and 2.59 for **PY-β-CPTCN**. These results are responsible for the stronger absorption of **PY-α-CPTCN** in the low-energy region. The potential energy surface scans of the model of end groups reveal that the adjacent end groups in **PY-α-CPTCN** have a lower rotational barrier and energy difference (ΔE) between the most stable and unstable form than those in **PY-β-CPTCN**, which makes the backbone of **PY-α-CPTCN** rotate more easily (Fig. S15). The large rotational barrier and ΔE of **PY-β-CPTCN** may be attributed to intramolecular hydrogen bonds between the O atom on the carbonyl group and the α-H atom on the thiophene of adjacent terminal units and steric constraints imposed by adjacent rigid fused rings.[38,39] According to the optimized molecular geometries shown in Fig. S16, the dihedral angles between the adjacent CPTCN units in **PY-α-CPTCN** and **PY-β-CPTCN** are calculated to be 14.52° and 1.58°, respectively. The smaller rotational barrier and the more twisted conformation of **PY-α-CPTCN** may foster energetic disorder, contributing to its broader absorption spectrum compared to **PY-β-CPTCN**.[40] Their frontier molecular orbital (FMO) distributions were further visualized by using Multiwfn and VMD software.[41,42] As shown in Fig. 4a and b, **PY-α-CPTCN** and **PY-β-CPTCN** both exhibit delocalized HOMO/LUMO distributions along the π-conjugated chains. Their HOMO distributions are mainly located on the fused-ring cores of SMA fragments and display similar patterns. However, the LUMO distributions are presented with different π-conjugation extension on the joint of two isomeric terminal units. **PY-α-CPTCN** holds a continuous π-bonding character between the two C atoms, ensuring the effective π-conjugation within the skeleton. Although **PY-β-CPTCN** also exhibits a delocalized LUMO orbital, the β-substituted pattern noticeably decreases the π-bonding character on the linked bond.[43] Moreover, the delocalization of electrons could be intuitively observed by electron localization function (ELF) (Fig. 4c and d).[44] It is evaluated by the equivalent surface surrounded by the iso-surface which decreases as the iso-value increases. At the joint of two CPTCN units, **PY-α-CPTCN** holds a continuous π-conjugation iso-surface until the iso-value is increased to 0.52, while the π-conjugation of **PY-β-CPTCN** was interrupted at the iso-value of 0.42. Thus, **PY-α-CPTCN** has stronger intramolecular π-conjugation effect than **PY-β-CPTCN**, which not only is consistent with the stronger and red-shifted absorption of **PY-α-CPTCN**, but also may facilitate more efficient charge transport.[45–48]

Based on the above results, the mechanism of PSMA-based photocatalytic systems could be proposed. During the process of light absorption, the electrons in PSMAs were excited to generate electron–hole pairs. The enhanced π-conjugation effect of **PY-α-CPTCN**, combined with the pull–push electronic interaction between donor and acceptor units, facilitates the efficient intramolecular charge delocalization and separation, underpinning its exceptional optoelectronic properties. When

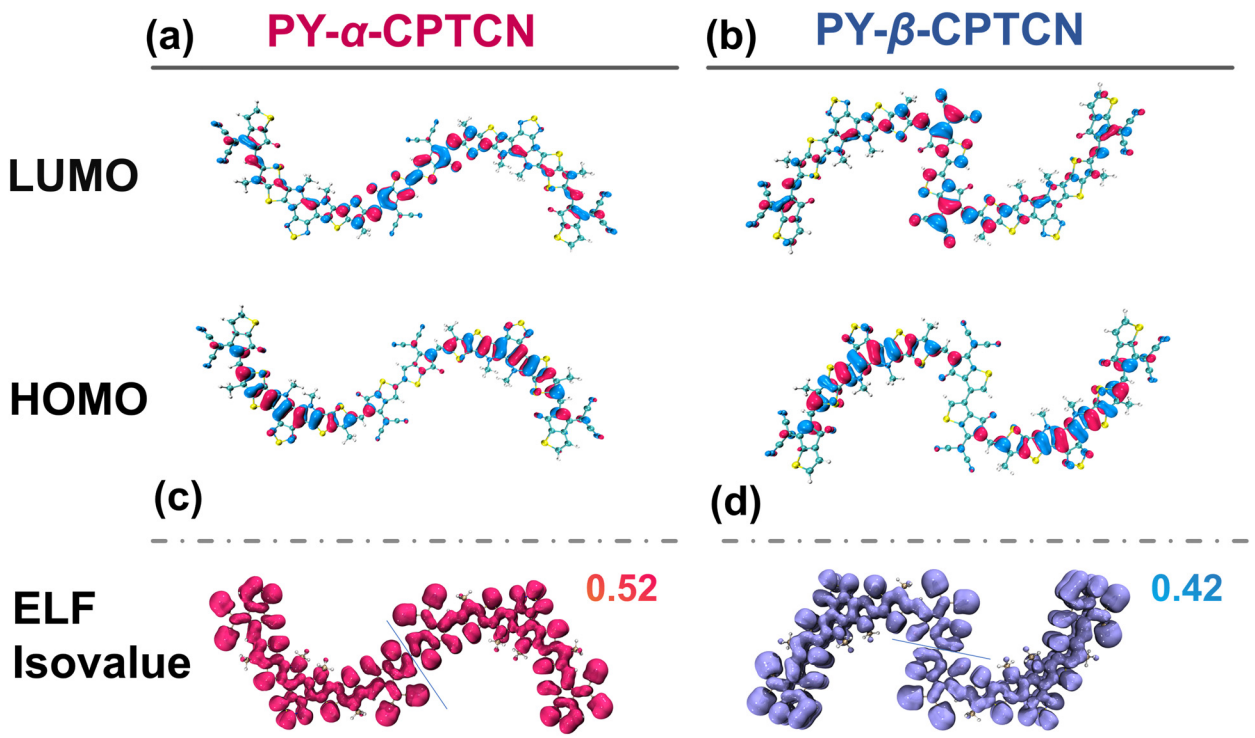

Fig. 4 (a and b) Frontier molecular orbital (FMO) distributions and (c and d) electron localization function (ELF) iso-values of **PY-α-CPTCN** and **PY-β-CPTCN**.

these photogenerated species migrate to the surface of NPs, the excited electrons would transfer to the cocatalyst Pt, and the holes were consumed by ascorbic acid to reduce the recombination of the electron–hole pairs. Finally, the H_2 evolution reaction was accomplished on the active catalytic sites which was afforded by the electron sink Pt.[49–51]

Conclusions

In summary, the isomerization strategy was adopted to construct two PSMA-based photocatalysts (**PY-α-CPTCN** and **PY-β-CPTCN**) featuring isomeric thiophene-fused terminal units. Comparative analysis reveals that **PY-α-CPTCN** NPs exhibit a significantly stronger and broader absorption spectrum in the visible and NIR region relative to **PY-β-CPTCN** NPs at the equivalent concentration. The photoelectrochemical and spectroscopic experiments suggest that **PY-α-CPTCN** facilitates more efficient exciton dissociation and charge transport. Therefore, the single-component nano-photocatalyst based on **PY-α-CPTCN** achieves a high hydrogen evolution rate (HER) of 252.2 mmol g^{-1} h^{-1}, representing a 3.2-fold enhancement over the **PY-β-CPTCN** catalyst (79.7 mmol g^{-1} h^{-1}). As revealed by the theoretical calculations, **PY-α-CPTCN** exhibits a stronger intramolecular π-conjugation effect, which is consistent with its more delocalized excited state, and ensures improved optical absorption as well as more efficient charge transport. These isomeric PSMAs, featuring precisely tunable π-conjugation, demonstrate the critical role of intramolecular delocalization of the excited state in photocatalytic hydrogen evolution. This insight advances the understanding of design principles for PSMA-based photocatalysts.

Conflicts of interest

There are no conflicts to declare.

Data availability

Supplementary information: Detailed synthesis route, TGA curves, cryo-TEM and SEM images, steady-state photoluminescence spectra, CV curves, photocatalytic hydrogen evolution test and so on. See DOI: **https://doi.org/10.1039/D5CY00775E**

The data that support the findings of this study are available from the corresponding author upon reason able request

Acknowledgements

This work was financially supported by the Ministry of Science and Technology of the People's Republic of China (the National Key R&D Program of China, No. 2022YFB4200400), the Strategic Priority Research Program of the Chinese Academy of Sciences (No. XDB0520102), and the National Natural Science Foundation of China (Grant No. 22075272, 22275182, 51973211, 51833009, 21674111 and 52261135541).

References

1 H. Song, S. Luo, H. Huang, B. Deng and J. Ye, *ACS Energy Lett.*, 2022, **7**, 1043–1065.
2 X. Tao, Y. Zhao, S. Wang, C. Li and R. Li, *Chem. Soc. Rev.*, 2022, **51**, 3561–3608.
3 Y. Guo, Q. Zhou, B. Zhu, C. Y. Tang and Y. Zhu, *EES Catal.*, 2023, **1**, 333–352.
4 D. Gunawan, J. Zhang, Q. Li, C. Y. Toe, J. Scott, M. Antonietti, J. Guo and R. Amal, *Adv. Mater.*, 2024, **36**, 2404618.
5 N. Fajrina and M. Tahir, *Int. J. Hydrogen Energy*, 2019, **44**, 540–577.
6 S. Chen, T. Takata and K. Domen, *Nat. Rev. Mater.*, 2017, **2**, 17050.
7 Y. Liu, B. Li and Z. Xiang, *Small*, 2021, **17**, 2007576.
8 C. Zhao, Z. Chen, R. Shi, X. Yang and T. Zhang, *Adv. Mater.*, 2020, **32**, 1907296.
9 R. J. Lyons and R. S. Sprick, *Mater. Horiz.*, 2024, **11**, 3764–3791.
10 G. Zhang, Z.-A. Lan and X. Wang, *Angew. Chem., Int. Ed.*, 2016, **55**, 15712–15727.
11 Y. Xu, T. Yan, N. Chen, H. Chen, A. Xue and X. Zhang, *Int. J. Hydrogen Energy*, 2024, **51**, 1417–1428.
12 Z. Yang, T. Bao, H. Liu, S.-T. Zhang, Z. Yang, S. Zhao, Z. Feng, P. She, L. Yao and B. Yang, *Int. J. Hydrogen Energy*, 2025, **126**, 178–184.
13 J. Zhan, X. Zhang, C. Zhang, Y. Yang, X. Ding, D. Ding, B. Chai, K. Dai and H. Chen, *Int. J. Hydrogen Energy*, 2024, **80**, 115–124.
14 Q. Wang and K. Domen, *Chem. Rev.*, 2020, **120**, 919–985.
15 L. Wang and W. Zhu, *Adv. Sci.*, 2024, **11**, 2307227.
16 Y. Chen, X. Luo, J. Zhang, L. Hu, T. Xu, W. Li, L. Chen, M. Shen, S.-B. Ren, D.-M. Han, G.-H. Ning and D. Li, *J. Mater. Chem. A*, 2022, **10**, 24620–24627.
17 M. H. Elsayed, M. Abdellah, A. Z. Alhakemy, I. M. A. Mekhemer, A. E. A. Aboubakr, B.-H. Chen, A. Sabbah, K.-H. Lin, W.-S. Chiu, S.-J. Lin, C.-Y. Chu, C.-H. Lu, S.-D. Yang, M. G. Mohamed, S.-W. Kuo, C.-H. Hung, L.-C. Chen, K.-H. Chen and H.-H. Chou, *Nat. Commun.*, 2024, **15**, 707.
18 J. Zhao, Y. Liu, R. An, Y. Fu, P. Wang, X. Wu, H. Tong and L. Wang, *Adv. Funct. Mater.*, 2025, **35**, 2421994.
19 Suman and S. P. Singh, *J. Mater. Chem. A*, 2019, **7**, 22701–22729.
20 D. Sorbelli, Y. Wu, Z. Bao and G. Galli, *J. Mater. Chem. A*, 2024, **12**, 25837–25849.
21 T. Wang, M. Chen, R. Sun and J. Min, *Chem*, 2023, **9**, 1702–1767.
22 T. Yang and C. Zhan, *Sci. China:Chem.*, 2023, **66**, 2513–2531.
23 Z. Luo, T. Liu, R. Ma, Y. Xiao, L. Zhan, G. Zhang, H. Sun, F. Ni, G. Chai, J. Wang, C. Zhong, Y. Zou, X. Guo, X. H. Lu, H. Chen, H. Yan and C. Yang, *Adv. Mater.*, 2020, **32**, 2005942.
24 H. Wang, H. Chen, W. Xie, H. Lai, T. Zhao, Y. Zhu, L. Chen, C. Ke, N. Zheng and F. He, *Adv. Funct. Mater.*, 2021, **31**, 2100877.
25 H. Chen, D. Li, M. Lin, Q. Wang, Y. Zou, J. Ran, Y. Xing and X. Long, *Adv. Mater.*, 2025, **37**, 2500063.
26 W. Zhang, M. Sun, J. Cheng, X. Wu and H. Xu, *Adv. Mater.*, 2025, **37**, 2500913.
27 Q. Wang, C. Wang, K. Zheng, B. Wang, Z. Wang, C. Zhang and X. Long, *Angew. Chem., Int. Ed.*, 2024, **63**, e202320037.
28 Y. Lin, J. Wang, Z.-G. Zhang, H. Bai, Y. Li, D. Zhu and X. Zhan, *Adv. Mater.*, 2015, **27**, 1170–1174.
29 D. Xie, T. Liu, W. Gao, C. Zhong, L. Huo, Z. Luo, K. Wu, W. Xiong, F. Liu, Y. Sun and C. Yang, *Sol. RRL*, 2017, **1**, 1700044.
30 N. Cui, X. Li, H. Yang, J. Feng, K. Hu, X. Jiang, H. Fan, Y. Wu and C. Cui, *ACS Appl. Polym. Mater.*, 2024, **6**, 2223–2231.
31 T. Wang, R. Sun, W. Wang, H. Li, Y. Wu and J. Min, *Chem. Mater.*, 2021, **33**, 761–773.
32 Z. Luo, T. Liu, Y. Xiao, T. Yang, Z. Chen, G. Zhang, C. Zhong, R. Ma, Y. Chen, Y. Zou, X. Lu, H. Yan and C. Yang, *Nano Energy*, 2019, **66**, 104146.
33 H. Fu, M. Zhang, Y. Zhang, Q. Wang, Z. a. Xu, Q. Zhou, Z. Li, Y. Bai, Y. Li and Z.-G. Zhang, *Angew. Chem., Int. Ed.*, 2023, **62**, e202306303.
34 H. Fu, J. Yao, M. Zhang, L. Xue, Q. Zhou, S. Li, M. Lei, L. Meng, Z.-G. Zhang and Y. Li, *Nat. Commun.*, 2022, **13**, 3687.
35 J. Kosco, S. Gonzalez-Carrero, C. T. Howells, T. Fei, Y. Dong, R. Sougrat, G. T. Harrison, Y. Firdaus, R. Sheelamanthula, B. Purushothaman, F. Moruzzi, W. Xu, L. Zhao, A. Basu, S. De Wolf, T. D. Anthopoulos, J. R. Durrant and I. McCulloch, *Nat. Energy*, 2022, **7**, 340–351.
36 C. R. Firth, C. Jeanguenat, V. Lutz-Bueno, V. Boureau and K. Sivula, *Adv. Energy Mater.*, 2024, 2403372.
37 T. Wang, M. Li, Y. Chen, X. Che, F. Bi, Y. Yang, R. Yang and C. Li, *ACS Catal.*, 2023, **13**, 15439–15447.
38 T.-J. Wen, Z.-X. Liu, Z. Chen, J. Zhou, Z. Shen, Y. Xiao, X. Lu, Z. Xie, H. Zhu, C.-Z. Li and H. Chen, *Angew. Chem., Int. Ed.*, 2021, **60**, 12964–12970.
39 Q. Wang, S. Böckmann, F. Günther, M. Streiter, M. Zerson, A. D. Scaccabarozzi, W. L. Tan, H. Komber, C. Deibel, R. Magerle, S. Gemming, C. R. McNeill, M. Caironi, M. R. Hansen and M. Sommer, *Chem. Mater.*, 2021, **33**, 2635–2645.
40 X. Shen, X. Lai, H. Lai, Y. Wang, H. Li, M. Ou and F. He, *Adv. Funct. Mater.*, 2024, **34**, 2404919.
41 W. Humphrey, A. Dalke and K. Schulten, *J. Mol. Graphics*, 1996, **14**, 33–38.
42 T. Lu and F. Chen, *J. Comput. Chem.*, 2012, **33**, 580–592.
43 X. Cai, J. Xue, C. Li, B. Liang, A. Ying, Y. Tan, S. Gong and Y. Wang, *Angew. Chem., Int. Ed.*, 2022, **61**, e202200337.
44 H. Zhuo, X. Li, J. Zhang, S. Qin, J. Guo, R. Zhou, X. Jiang, X. Wu, Z. Chen, J. Li, L. Meng and Y. Li, *Angew. Chem., Int. Ed.*, 2023, **62**, e202303551.
45 S. Meng, Y. Zang, Z. Wang, H. Fu, M. Zhang, J. Yao, Q. Wang, H. Wang, Y. Yi, L. Xue, E. Zhou and Z.-G. Zhang, *Adv. Funct. Mater.*, 2025, **35**, 2423774.
46 S. Prodhan, S. Giannini, L. Wang and D. Beljonne, *J. Phys. Chem. Lett.*, 2021, **12**, 8188–8193.
47 A. J. Sneyd, D. Beljonne and A. Rao, *J. Phys. Chem. Lett.*, 2022, **13**, 6820–6830.
48 H. Zhuo, X. Li, J. Zhang, C. Zhu, H. He, K. Ding, J. Li, L. Meng, H. Ade and Y. Li, *Nat. Commun.*, 2023, **14**, 7996.
49 Y. Liu, J. Wu and F. Wang, *Appl. Catal., B*, 2022, **307**, 121144.
50 Y. Zhu, Z. Zhang, W. Si, Q. Sun, G. Cai, Y. Li, Y. Jia, X. Lu, W. Xu, S. Zhang and Y. Lin, *J. Am. Chem. Soc.*, 2022, **144**, 12747–12755.
51 S. Fang, L. Su, D. Sun and G. Zhang, *ACS Appl. Polym. Mater.*, 2024, **6**, 13253–13259.